

MIT Open Access Articles

*Salicylate Method for Ammonia Quantification
in Nitrogen Electroreduction Experiments:
The Correction of Iron III Interference*

The MIT Faculty has made this article openly available. **Please share**
how this access benefits you. Your story matters.

Citation: Giner-Sanz, Juan José, Leverick, Graham M, Pérez-Herranz, Valentín and Shao-Horn, Yang. 2020. "Salicylate Method for Ammonia Quantification in Nitrogen Electroreduction Experiments: The Correction of Iron III Interference." *Journal of the Electrochemical Society*, 167 (13).

As Published: 10.1149/1945-7111/ABBDD6

Publisher: The Electrochemical Society

Persistent URL: <https://hdl.handle.net/1721.1/139773>

Version: Final published version: final published article, as it appeared in a journal, conference proceedings, or other formally published context

Terms of use: Creative Commons Attribution 4.0 International license



OPEN ACCESS

Salicylate Method for Ammonia Quantification in Nitrogen Electroreduction Experiments: The Correction of Iron III Interference

To cite this article: Juan José Giner-Sanz *et al* 2020 *J. Electrochem. Soc.* **167** 134519

View the [article online](#) for updates and enhancements.



Element Six is a world leader in the development and production of synthetic diamond solutions




Since 1959, our focus has been on engineering the properties of synthetic diamond to unlock innovative applications, such as thermal management, water treatment, optics, quantum and sensing. Our patented technology places us at the forefront of synthetic diamond innovation, enabling us to deliver competitive advantage to our customers through diamond-enabled solutions.

Find out more and contact the team at:
ustechologies@e6.com

   e6.com



Salicylate Method for Ammonia Quantification in Nitrogen Electroreduction Experiments: The Correction of Iron III Interference

Juan José Giner-Sanz,^{1,2}  Graham M. Leverick,^{3,*}  Valentín Pérez-Herranz,^{2,z} and Yang Shao-Horn^{1,3,4,**,z} 

¹Research Laboratory of Electronics, Massachusetts Institute of Technology, Cambridge, Massachusetts 02139, United States of America

²IEC group, Depto. Ingeniería Química y Nuclear, Universitat Politècnica de València, Valencia 46022, Spain

³Department of Mechanical Engineering, Massachusetts Institute of Technology, Cambridge, Massachusetts 02139, United States of America

⁴Department of Materials Science and Engineering, Massachusetts Institute of Technology, Cambridge, Massachusetts 02139, United States of America

The salicylate method is one of the ammonia quantification methods that has been extensively used in literature for quantifying ammonia in the emerging field of nitrogen (electro)fixation. The presence of iron in the sample causes a strong negative interference on the salicylate method. Today, the recommended method to deal with such interferences is the experimental correction method: the iron concentration in the sample is measured using an iron quantification method, and then the corresponding amount of iron is added to the calibration samples. The limitation of this method is that when a batch of samples presents a great iron concentration variability, a different calibration curve has to be obtained for each sample. In this work, the interference of iron III on the salicylate method was experimentally quantified, and a model was proposed to capture the effect of iron III interference on the ammonia quantification result. This model can be used to correct the iron III interferences on ammonia quantification. The great advantage of this correction method is that it only requires three experimental curves in order to correct the iron III interference in any sample provided the iron III concentration is below the total peak suppression concentration.

© 2020 The Author(s). Published on behalf of The Electrochemical Society by IOP Publishing Limited. This is an open access article distributed under the terms of the Creative Commons Attribution 4.0 License (CC BY, <http://creativecommons.org/licenses/by/4.0/>), which permits unrestricted reuse of the work in any medium, provided the original work is properly cited. [DOI: 10.1149/1945-7111/abbdd6]



Manuscript submitted August 30, 2020; revised manuscript received September 23, 2020. Published October 15, 2020.

Supplementary material for this article is available [online](#)

List of sybools

Roman symbols

A_{λ}	Absorbance at wavelength λ
A_{λ}^*	Normalized absorbance at wavelength λ
C	Molar concentration ($\text{mol} \cdot \text{m}^{-3}$)
e	Relative error
l	Optical path (m)
R^2	Determination coefficient

Greek symbols

β	Background coefficient
ϵ^*	Effective molar attenuation coefficient ($\text{m}^3 \cdot \text{mol}^{-1} \cdot \text{m}^{-1}$)
Γ	Interference coefficient
λ	Wavelength (m)

Subscripts

TAN	Total ammonia nitrogen (i.e. $\text{NH}_3 + \text{NH}_4^+$)
-----	--

Superscripts

Final	In the final mixture (i.e. after the reagent additions)
Sample	In the initial sample (i.e. before the reagent additions)

There has been a rapidly growing interest in the development of electrochemical methods for synthesizing fuels and chemicals, motivated by the dream of a global shift towards sustainable energy and feedstocks.^{1–3} In this context, nitrogen fixation as ammonia is viewed as a key process,^{4–7} since ammonia synthesis is considered as one of the foundational chemical processes of the human

society,^{8–10} supporting approximately 27% of the world's population over the past century.^{11,12}

Since French historian and chemist, Marcellin Pierre Eugène Berthelot, observed in 1859 the formation of a blue-colored dye when ammonia, phenol and hypochlorite were mixed,^{13,14} a great number of studies have investigated this reaction, which is known nowadays as the Berthelot or indophenol reaction.¹⁵ This term has since been generalized to refer to any reaction in which a phenolic compound reacts with ammonia and a hypochlorite source to form an indophenol-like dye, where the family of dyes is characterized by the indophenol group. This highly conjugated group strongly absorbs visible light in the range between 630 nm and 720 nm. This family of reactions has been used widely for ammonia quantification using ultraviolet-visible (UV-vis) spectroscopy,^{16–18} and in situ sensors.^{19–21}

The salicylate method is a modification of the indophenol method, in which sodium salicylate is used as the phenolic compound, sodium hypochlorite is used as the hypochlorite source, and sodium nitroprusside is used as a catalyst. The salicylate method has been used extensively in a wide range of applications including aqueous samples,²² non-aqueous samples,²³ air samples,²⁴ soil samples,²⁵ (micro)biological samples,²⁶ pervaporation samples,²⁷ and acidic digests of vegetal materials.²⁸ More recently, this method has been employed to quantify the ammonia produced during (electrochemical) nitrogen reduction experiments.^{29,30} The use of sodium salicylate in the method avoids working with phenol (poisonous and volatile),^{31,32} and the generation of the toxic fumes (ortho-chlorophenol) that are produced during the indophenol method.³³ In the salicylate method, the amount of ammonia in a sample can be determined by converting the ammonia contained in the sample into an intense blue indophenol-like dye, which can then be quantified by UV-Visible spectrometry.^{34,35}

Unfortunately, the salicylate method is sensitive to the presence of a large variety of interferents in the sample,¹⁵ which can lead to

*Electrochemical Society Student Member.

**Electrochemical Society Fellow.

^zE-mail: vperez@iqn.upv.es; shaohorn@mit.edu

false positives (i.e. positive interferents) or to underestimated results (i.e. negative interferents). Moreover, the salicylate method is able to detect such low ammonia concentrations, that the cross-contamination of the samples with the ammonia present in the laboratory environment and in the elements of the experimental setup (v.g. membrane, catalyst, etc...) can cause false positive results in nitrogen fixation experiments, due to the small amount of ammonia typically produced in such experiments. Nowadays, it is well established that adventitious contamination and interferences on the ammonia quantification method are two of the main reasons of the non-reproducibility of the results of many works of the nitrogen (electro)reduction field.⁴ In order to ensure that the detected ammonia has really been produced by dinitrogen (electro)reduction, and does not come from adventitious contamination or ammonia quantification interference, rigorous protocols based on ¹⁵N isotopic labelling have been proposed. One of such protocols is the protocol proposed by Prof. Chorkendorff's group.⁴ The main limitation of isotopic labelling methods is their high cost. For this reason, the salicylate method is still widely used for initial screening nitrogen (electro)reduction experiments, which then are validated using ¹⁵N isotopic labelling. Although the screening experiments have to be validated using isotopic methods, it is highly recommended to reduce the experimental error in the screening experiments as much as possible. One way to achieve this is to identify the presence of possible interferents in the samples and, if possible, to correct the effect of those interferents on the ammonia quantification results.

A common example of interferent on the salicylate method is iron: the presence of its ions in the sample interferes with the quantification method.^{33,36–38} For instance, the Hach Company lists iron as one of the main interferents in all its ammonia quantification tests based on the salicylate method. In fact, the Hach Company's protocols state that iron interferes with the salicylate method at all concentration levels. While this interference phenomenon is empirically known, few methods are established to address the iron interference on the salicylate method. The traditional strategy to deal with iron interferences on the salicylate method is to measure the iron concentration in the sample using a total iron concentration quantification method, and then add the corresponding amount of iron to the calibration samples.³⁹ In this way, the iron effect on the ammonia quantification is corrected experimentally. However, in some applications, the iron concentration is not constant from one sample to another, within a batch of samples. In such applications, the experimental correction method requires the preparation of a different absorbance-versus-ammonia concentration calibration curve for each one of the different iron concentrations. The number of required calibration curves can be large, especially in experiments with iron concentrations varying over a wide range of values. For instance, this is the case in nitrogen fixation experiments in which iron based catalysts are used. Such catalysts have been extensively used in the nitrogen fixation field,⁴⁰ and many examples can be found in literature, including metallic iron,⁴¹ nanostructured iron-based electrocatalysts,⁴² Ni-doped iron catalysts,⁴³ iron oxides,⁴⁴ and Mo-doped FeS₂ catalysts.⁴⁵ In these systems, iron leaching from the catalyst to the electrolyte can cause the iron concentration in the electrolyte to increase over time.

In this work, the interference of iron III on the ammonia quantification peak in the salicylate method was experimentally quantified, and an empirical model was developed to model the effect of the iron III interference on the ammonia quantification in the salicylate method. This model can be used to correct *a posteriori* the iron III interference effect on the ammonia quantification results.

Experimental Methods

Materials.—Ammonium chloride (Sigma-Aldrich, ACS Grade) was used as received. Sodium salicylate (Ensure Millipore, for analysis), sodium nitroprusside dihydrate (Ensure Millipore, for analysis), sodium citrate dihydrate (Ensure Millipore, for analysis),

sodium hydroxide (Sigma-Aldrich, anhydrous, free-flowing pellets ACS reagent) and the sodium hypochlorite aqueous solution (Sigma-Aldrich, reagent grade, available chlorine 4.00%–4.99%) were used as received. Iron (III) chloride hexahydrate (Sigma-Aldrich, ACS Grade) was used as received. All the reagents were stored at room temperature, except the sodium hypochlorite aqueous solution, which was stored at 5 °C. Water was obtained from a Millipore system (Resistivity: 18.2 MΩ·cm at 25 °C; TOC: 4 ppb), and was always freshly prepared just before its use.

The samples were stored and manipulated in scintillation vials (SciLabware, 20 ml). 3 ml disposable methacrylate cuvettes (VWR, 1 cm optical path) were used for UV–Visible measurements. A GENESYS® 180 UV–Visible spectrophotometer was used to measure the UV–Visible spectra.

The salicylate method.—Nowadays, there are several variants of the salicylate method available in literature. In this work, a modified version of the method originally proposed by Bower and Holm-Hansen⁴⁶ and reproduced by Le and Boyd,⁴⁷ was used.

Three reagent solutions were prepared: the salicylate catalyst solution (Solution S1), the alkaline citrate solution (Solution S2), and the alkaline hypochlorite solution (Solution S3). Solution S1 was prepared by dissolving sodium salicylate powder and sodium nitroprusside dihydrate flakes in freshly prepared Millipore water in order to obtain a 2.75 M sodium salicylate and 0.95 mM sodium nitroprusside solution. Solution S2 was prepared by dissolving sodium citrate dihydrate powder and sodium hydroxide pellets in order to obtain a 340 mM sodium citrate and 465 mM sodium hydroxide solution. Finally, solution S3 was obtained by mixing 10 vol% of commercial 5% sodium hypochlorite aqueous solution with solution S2. Solutions S1 and S3 were not stored and were always freshly prepared just before analyzing the samples. On the contrary, solution S2 was prepared in advanced, and stored at room temperature. Furthermore, solution S1 was kept in an opaque dark bottle during the whole analysis process.

To analyze a given sample: 5 ml of sample were mixed with 600 μl of solution S1, and mixed vigorously. Then, 1 ml of solution S3 was added to the aforementioned mixture, and mixed thoroughly. This addition was performed in the dark. After that, the sample was stored in the dark for 1 h, after which its visible spectra was measured using a double beam spectrophotometer. Since the salicylate reagents (especially sodium nitroprusside) have color (Fig. S1 is available online at stacks.iop.org/JES/167/134519/mmedia), a blank sample was prepared by applying the aforementioned addition protocol to 5 ml of freshly prepared Millipore® water. This developed blank sample was used as blank and reference sample during the UV–Visible measurement of the different samples. Both, the sample preparation and measurement, were done at ambient temperature. All the visible spectra were measured from 850 nm to 350 nm, with a step size of 0.5 nm and a sweep speed of 5 nm · s^{−1}.

Absorbance-versus-ammonia concentration calibration curves.—

First of all, for the iron free calibration curve, a parent solution of 0.8 mM Total Ammonia Nitrogen (TAN, i.e. $\text{NH}_3 + \text{NH}_4^+$), was prepared by dissolving solid NH_4Cl powder in freshly prepared Millipore® water. A set of solutions of different TAN concentrations (in the linearity region) were prepared by successive dilutions of the parent solution, using freshly prepared Millipore® water. This set of solutions was analyzed using the salicylate method protocol described above.

For the calibration curves in the presence of Fe III, the same procedure was used with the only difference that instead of using Millipore® water to prepare the NH_4Cl parent solution and its corresponding daughter dilutions; an Fe III solution of the corresponding concentration was used for this matter. The different Fe III solutions were prepared by dissolving the required amount of $\text{FeCl}_3 \cdot 6\text{H}_2\text{O}$ in freshly prepared Millipore® water.

Background and interference measurements.—First of all, an ammonium parent solution of 1.5 mM TAN was prepared by dissolving solid NH_4Cl in freshly prepared Millipore® water. Then, a 0.1 M iron parent solution was prepared by solid $\text{FeCl}_3 \cdot 6\text{H}_2\text{O}$ in freshly prepared Millipore® water. For background measurements, 5 ml samples of different Fe III concentrations were prepared by diluting accordingly the iron parent solution using freshly prepared Millipore® water. For the interference measurements, 5 ml samples of different Fe III concentrations and a given TAN concentration were prepared by mixing the required amounts of iron and ammonium parent solutions, and then diluting accordingly using freshly prepared Millipore® water. Following this procedure, the ammonia concentration is the same in all the prepared samples (zero concentration for the background measurement samples, and a non-zero concentration for the interference measurement samples). What changes from sample to sample is the Fe III concentration.

The different sets of samples were analyzed using the salicylate method protocol described above. The order in which the reagents were added to the samples within a given set of samples (and therefore, the order in which the UV–Visible spectra were measured) was random (i.e. neither in increasing or decreasing Fe III concentration order); except for the blank sample, which was left at the end of the addition queue. This randomization strategy was used in order to orthogonalize the interferent concentration factor from the order factor. This is important to avoid confusing order effects (v.g. time drifts) with concentration effects. For instance, if there was a time drift in the system, and the samples were measured in increasing concentration order, then the effect of the time drift would be attributed to the concentration (erroneously). On the contrary, measuring in random order, ensures that any trend observed is actually due to the interferent concentration effect.

Salicylate-iron III titration measurements.—First, a 2.5 mM KOH solution and a 30 mM $\text{FeCl}_3 \cdot 6\text{H}_2\text{O}$ solution were prepared using freshly prepared Millipore® water. Next, the 2.5 mM KOH solution was used to dissolve 10 mM sodium salicylate to create a 10 mM sodium salicylate + 2.5 mM KOH solution. 1 ml of the 10 mM sodium salicylate + 2.5 mM KOH solution was pipetted into a 3 ml methacrylate cuvette (VWR, 1 cm optical path) and UV–Visible spectra were collected with Millipore® water as the blank and reference samples. Next, the 30 mM $\text{FeCl}_3 \cdot 6\text{H}_2\text{O}$ solution was added to the cuvette in 50 μl increments to obtain the spectra for 0.15, 0.30 and 0.45 ratios of $C_{\text{Fe III}}/C_{\text{NaSal}}$. To avoid the signal saturating the spectrophotometer detector, two new solutions were prepared by diluting the sodium salicylate and $\text{FeCl}_3 \cdot 6\text{H}_2\text{O}$ solutions by a factor of 3 with Millipore® water to obtain 3.33 mM sodium salicylate + 0.833 mM KOH and 10 mM $\text{FeCl}_3 \cdot 6\text{H}_2\text{O}$ solutions. 1 ml of the 3.33 mM sodium salicylate + 0.833 mM KOH solution and 0.1 ml of the 10 mM $\text{FeCl}_3 \cdot 6\text{H}_2\text{O}$ were added to a new methacrylate cuvette to replicate the 0.30 $C_{\text{Fe III}}/C_{\text{NaSal}}$ UV–vis spectra and confirm that dilution did not alter the spectra. Finally, the 10 mM $\text{FeCl}_3 \cdot 6\text{H}_2\text{O}$ solution was added to the cuvette in 50 μl increments to obtain the spectra for 0.60, 0.75, 0.90, 1.05, 1.20 and 1.35 ratios of $C_{\text{Fe III}}/C_{\text{NaSal}}$.

Results and Discussion

Absorbance-versus-ammonia concentration calibration curves.—The experimental UV–visible spectra (Figs. 1a and 1b) obtained when the salicylate method was applied to the water calibration samples (i.e. different TAN concentrations in water) and to the 20 mM Fe III calibration samples (i.e. different TAN concentrations in 20 mM Fe III solution), display the characteristic indophenol peak at 652 nm in samples with and without Fe III. This peak can be attributed to the indophenol-type dye formed after adding the salicylate method reagents (i.e. the salicylate catalyst solution and the alkaline hypochlorite solution) to the sample. In addition, the presence of Fe III generates

a new spectrum feature below 550 nm, where for an Fe III concentration of 20 mM, this feature presents large absorption that saturates the instrument. The new feature can be attributed to the formation of $\text{Fe}(\text{OH})_3$ and Fe-Salicylate complex(es) (most likely a 1:1 complex, see section 2 of the supplementary information) when the reagents of the salicylate method were added to the sample.

The presence of Fe III did not cause a hypsochromic shift nor a bathochromic shift of the 652 nm peak of the indophenol-type dye, since the peak position did not change in Fig. 1b. However, the presence of Fe III in the samples did lead to a hypochromic shift in the intensity of the peak at 652 nm, where increasing Fe III concentration decreased the peak height for a given TAN concentration. For instance, for a 0.14 mM TAN concentration sample, the 652 nm peak absorbance is around 2.4 when no Fe III is present in the sample, and is around 1.8 when the sample contains 20 mM of Fe III. This hypochromic shift of the 652 nm peak was found to considerably reduce the effective molar attenuation coefficient when Fe III was present in the sample, from $17.4 \text{ mM}^{-1} \cdot \text{cm}^{-1}$ in pure water to $12.0 \text{ mM}^{-1} \cdot \text{cm}^{-1}$ in the 20 mM Fe III solution, which would translate to a 45% error in the ammonia quantification if the calibration curve in water was used in the latter case. This strong negative interference of Fe III on the indophenol peak generation in the salicylate method is consistent with previous reports.³⁹ Therefore, a model is needed to systematically correct the influence of Fe III on the quantification of ammonia in samples containing Fe III using the salicylate method.

The observation that the presence of Fe III in the sample causes a hypochromic shift, but does not cause a hypsochromic shift nor a bathochromic shift (i.e. it reduces the peak absorbance but does not change its position), suggests that the reduction of the effective molar attenuation coefficient (i.e. combination of the dye production yield and the dye molar attenuation coefficient) when Fe III is present, is due to a reduction of the dye production yield; and that the dye molar attenuation coefficient does not change when Fe III is present (i.e. the presence of Fe III does not change the structure of the formed dye).

pH measurements of the samples with no ammonia after the salicylate method showed decreasing pH with increasing Fe III content (Fig. S6). Considering that Fe III can form stable precipitates with OH^- (with a solubility product constant of $K_{sp} = 2.79 \cdot 10^{-39}$),⁴⁸ we propose that the lower dye production yield when Fe III is present is caused by the sequestration of the OH^- ions added with reagent S3, by Fe III ions to form $\text{Fe}(\text{OH})_3$. This hypothesis is supported by previous reports showing that the dye formation yield can be highly pH dependent.^{15,49} As shown in Krom's work,⁵⁰ the peak absorbance is reduced significantly (i.e. nearly halved) when the dye is formed at pH 10 in comparison to when the dye formation reaction takes place at pH 12. As shown in section 3 of the supplementary information, when the sample contained 20 mM of Fe III, the reaction pH was 11.5; and when the sample contained 40 mM of Fe III, the reaction pH was 8. The reduction of the free OH^- ions in the reaction mixture causes that the dye formation reaction takes place at a lower pH, which lowers the dye production yield, causing the observed negative interference of Fe III on the salicylate method.

Modelling the interference of Fe III on the salicylate method.

The absorbance-versus-TAN concentration calibration curves (Fig. 1c) were linear for both, samples containing 0 mM Fe III ($R^2 = 99.94\%$) and samples containing 20 mM Fe III ($R^2 = 99.68\%$). This fact provides the physical basis for the traditional method of correction for the Fe III interference on the ammonia quantification by the salicylate method (i.e. the experimental correction method). As seen in Fig. 1c, the presence of Fe III has two effects on the calibration curve of absorbance at 652 nm vs TAN concentration: 1) Fe III causes nonzero background absorbance at 652 nm, leading to increasing vertical translation of the calibration curve with increasing Fe III concentrations, and 2) Fe III generates a negative interference causing a reduction in the slope of the calibration curve.

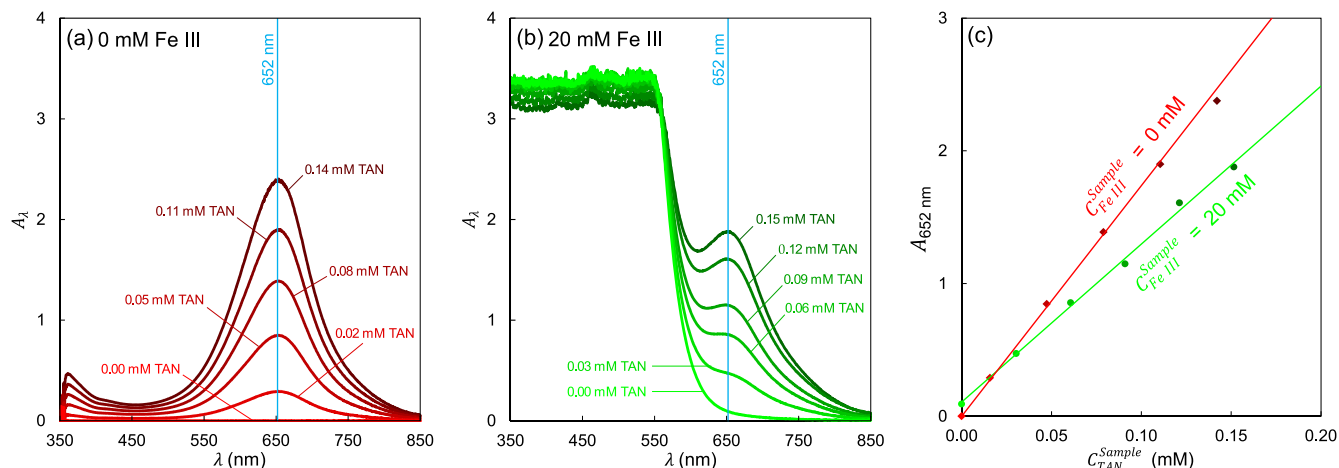


Figure 1. UV–Visible spectra (i.e. absorbance, A_λ ; as a function of wavelength, λ) obtained using the salicylate method on (a) the water calibration samples (i.e. different TAN concentrations in water) and on (b) the 20 mM Fe III calibration samples (i.e. different TAN concentrations in 20 mM Fe III solution). In all cases, the spectra were measured against the reference sample, from 850 nm to 350 nm with a step size of 0.5 nm and a sweep speed of $5 \text{ nm} \cdot \text{s}^{-1}$. (c) The 652 nm peak calibration curves obtained by representing the absorbance at 652 nm ($A_{652 \text{ nm}}$) of the spectra in sub figures (a) and (b), as a function of the TAN concentration in the sample ($C_{\text{TAN}}^{\text{Sample}}$). The dots correspond with the experimental points, while the lines are the fitted linear regression lines. From the slopes of the fitted lines, and the optic path of the used cuvettes ($l = 1 \text{ cm}$), the effective molar attenuation coefficient were determined: for the water calibration, $\varepsilon^* = 17.4 \text{ mM}^{-1} \cdot \text{cm}^{-1}$ ($R^2 = 99.94\%$); and for the 20 mM Fe III calibration, $\varepsilon^* = 12.0 \text{ mM}^{-1} \cdot \text{cm}^{-1}$ ($R^2 = 99.68\%$).

The linearity of the calibration curves in Fig. 1c implies that both, the background and the interference effect, are not dependent on the ammonia concentration. Assuming that the background and interference coefficients only depend on the Fe III concentration, and do not depend on the ammonia concentration, the interferences of Fe III on the salicylate method can be modelled using the following multiplicative interference with background model:

$$A_{652 \text{ nm}}(C_{\text{TAN}}^{\text{Sample}}, C_{\text{Fe III}}^{\text{Sample}}) = l \cdot \varepsilon_{652 \text{ nm}}^*(C_{\text{Fe III}}^{\text{Sample}} = 0) \cdot \Gamma(C_{\text{Fe III}}^{\text{Sample}}) \cdot C_{\text{TAN}}^{\text{Sample}} + \beta(C_{\text{Fe III}}^{\text{Sample}}) \quad [1]$$

Where $C_{\text{TAN}}^{\text{Sample}}$ and $C_{\text{Fe III}}^{\text{Sample}}$ are the concentration of TAN and Fe III in the sample, respectively, $A_{652 \text{ nm}}$ is the absorbance at 652 nm, l is the light optic path, and $\varepsilon_{652 \text{ nm}}^*(C_{\text{Fe III}}^{\text{Sample}} = 0)$ is the effective molar attenuation coefficient when no Fe III is present (related to the slope of the calibration curve in water samples). β denotes the background coefficient which is associated to the background color due to the formation of $\text{Fe}(\text{OH})_3$ and Fe-salicylate complexes with Fe III presence. Γ represents the interference coefficient, which captures the effect of Fe III on reducing the dye formation yield (thus reducing the effective molar attenuation coefficient). This interference coefficient is a dimension-less coefficient that quantifies the magnitude of the interference. In the case of no interference, $\Gamma = 1$. Since Fe III causes a hypochromic interference (i.e. negative interference), in this case $\Gamma \leq 1$. The greater interference, more deviation of Γ from 1.

Background and interference coefficients.—In the case where the sample does not contain ammonia, Eq. 1 can be reduced to the following:

$$A_{652 \text{ nm}}(C_{\text{TAN}}^{\text{Sample}} = 0; C_{\text{Fe III}}^{\text{Sample}}) = \beta(C_{\text{Fe III}}^{\text{Sample}}) \quad [2]$$

Consequently, the background coefficient associated to a given Fe III concentration can be experimentally obtained by measuring the absorbance at 652 nm of a sample analyzed by the salicylate method, which contains the corresponding Fe III concentration and no ammonia (Fig. 2a). The experimentally determined background coefficients were relatively low since the absorbance at 652 nm is due to the tail of a spectrum feature that appears at lower wavelengths (i.e. in the 350–550 nm range), that causes the

instrument to saturate at those wavelengths (Fig. S4). This spectrum feature increases with Fe III concentration, and its tail enlarges towards higher wavelengths, causing the background coefficient to increase with Fe III concentration. This observation is consistent with the hypothesis that the background comes from the formation of $\text{Fe}(\text{OH})_3$ and Fe-salicylate complexes, and therefore, at higher Fe III concentration the background increases. The increase in the background coefficient with the Fe III concentration was found to be nonlinear, where the rate of increase first decreased and then increased (inset of Fig. 2a). This nonlinear changes in the background coefficient with Fe III concentration can be attributed to light scattering by the formed insoluble species and to the pH changes of the final mixture (section 3 of the supplementary information), which shift the chemical equilibria responsible for the background generation (between $\text{Fe}(\text{OH})_3$ and Fe-salicylate complexes) and the position of the 350 nm–550 nm spectrum feature. Although the spectrum feature cannot be entirely observed, since the instrument saturates, its position shift can be identified in Fig. 2a. This position shift is responsible for the complex evolution of the background coefficient with the Fe III concentration in the sample, instead of an evolution consistent with the Beer–Lambert law (i.e. linear evolution).

Clearing the interference coefficient from Eq. 1, the following expression can be obtained:

$$\Gamma(C_{\text{Fe III}}^{\text{Sample}}) = \frac{A_{652 \text{ nm}}(C_{\text{TAN}}^{\text{Sample}}, C_{\text{Fe III}}^{\text{Sample}}) - \beta(C_{\text{Fe III}}^{\text{Sample}})}{l \cdot \varepsilon_{652 \text{ nm}}^*(C_{\text{Fe III}}^{\text{Sample}} = 0) \cdot C_{\text{TAN}}^{\text{Sample}}} \quad [3]$$

$$= \frac{A_{652 \text{ nm}}(C_{\text{TAN}}^{\text{Sample}}, C_{\text{Fe III}}^{\text{Sample}}) - \beta(C_{\text{Fe III}}^{\text{Sample}})}{A_{652 \text{ nm}}(C_{\text{TAN}}^{\text{Sample}}, C_{\text{Fe III}}^{\text{Sample}} = 0)}$$

Therefore, in order to determine experimentally the interference coefficient for a given Fe III concentration, the 652 nm absorbance containing the corresponding Fe III and TAN concentrations, and the 652 nm absorbance containing the same TAN concentration but no Fe III, are required. In order to quantify the interference coefficients at different Fe III concentrations, an interference experiment was required. Such experiment consists in preparing a set of samples with the same TAN concentration and different Fe III concentrations, and applying to them the salicylate method.

For a given TAN concentration, when the Fe III concentration increases, a peak at 422 nm grows (until it reaches saturation) (Fig. 2b). This peak, associated with the background compounds

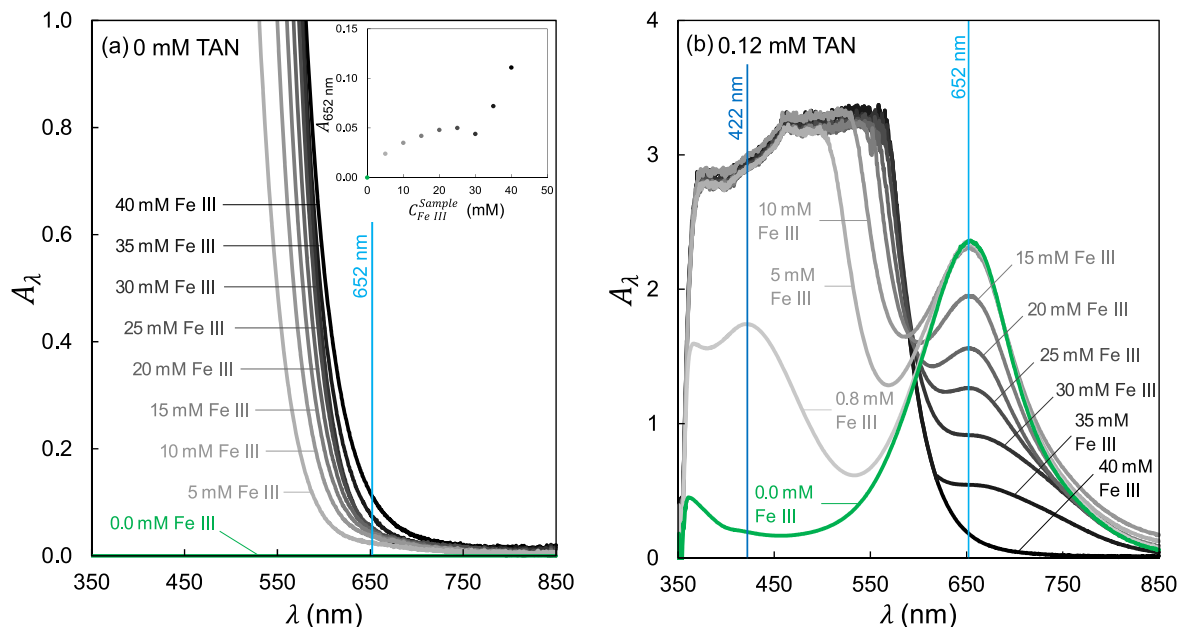


Figure 2. Effect of the Fe III concentration in the sample on the UV–Visible spectra obtained by the salicylate method, for a given TAN concentration. UV–Visible spectra (i.e. absorbance, A_λ ; as a function of wavelength, λ) obtained using the salicylate method on samples with different Fe III concentrations, and a given TAN concentration: (a) $C_{TAN}^{Sample} = 0$ mM, (b) $C_{TAN}^{Sample} = 0.12$ mM. In all cases, the spectra were measured against the reference sample, from 850 nm to 350 nm with a step size of 0.5 nm and a sweep speed of $5 \text{ nm} \cdot \text{s}^{-1}$. Inset in sub figure (a): the absorbance at 652 nm ($A_{652 \text{ nm}}$) of the spectra in sub figure (a) as a function of the Fe III concentration in the sample ($C_{Fe \text{ III}}^{Sample}$).

(i.e. $\text{Fe}(\text{OH})_3$ and $\text{Fe}:\text{Salicylate}$ complexes), corresponds to the saturated spectrum feature mentioned during the background coefficient discussion. Furthermore, for a given TAN concentration, when the Fe III concentration increases, the peak at 652 nm (i.e. the one used for ammonia quantification) is not affected by low Fe III concentrations and shrinks for high Fe III concentrations (Fig. 2b).

The interference experiment data (Fig. 2b) were used to calculate the interference coefficient at each Fe III concentration, using Eq. 2 with the corresponding experimentally determined background coefficient (Fig. 2a). Two distinct trends with the Fe III concentration can be identified in the interference coefficients determined experimentally (Fig. 3a). For low Fe III concentrations (i.e. below a threshold concentration), the presence of Fe III does not have any effect (i.e. $\Gamma = 1$) on the peak at 652 nm (i.e. the peak used for quantification). In contrast, for high Fe III concentrations (i.e. above a threshold concentration), an increase in the Fe III concentration causes a decrease of the 652 nm peak height. In this Fe III concentration range, there is a linear relation between the interference coefficient and the Fe III concentration in the sample.

Based on these observations, the following empirical model with 2 fitting parameters (δ and $C_{threshold}$) was proposed in order to capture the effect of the Fe III concentration on the interference coefficient:

$$\Gamma(C_{Fe \text{ III}}^{Sample}) = \begin{cases} 1 & \text{if } C_{Fe \text{ III}}^{Sample} \leq C_{threshold} \\ 1 + \delta \cdot (C_{threshold} - C_{Fe \text{ III}}^{Sample}) & \text{if } C_{Fe \text{ III}}^{Sample} > C_{threshold} \end{cases} \quad [4]$$

The above model was fitted to the interference coefficient experimental data (Fig. 3a). The fitted model perfectly captures the experimental effect of the Fe III concentration on the interference coefficient (and thus on the quantification peak), as shown by the very high determination coefficient of the fitted model ($R^2 = 99.90\%$), and the very good agreement between the predictions of the model and the experimental interference coefficients.

Even though the proposed model is an empirical model, its parameters have a clear meaning: parameter δ quantifies the interference effect magnitude; and parameter $C_{threshold}$ corresponds to the threshold Fe III concentration, below which there is no interference. In this case, the threshold interference is around 9 mM, suggesting no interference of Fe III on the ammonia quantification peak of the salicylate method at Fe III concentrations below 9 mM. This result is consistent with the mechanism hypothesized previously. As the final pH with 10 mM of Fe III is 11.95, close to the optimum value of 12, for Fe III concentrations lower than 10 mM, the reaction pH will be high enough not to affect the dye production yield, and therefore not producing interference with the salicylate method.

It should be noted that even if the empirical model predicts negative interference coefficients for Fe III concentrations above 42 mM (Fig. 3a), these values have no physical meaning. The Fe III concentration that leads to a zero interference coefficient ($\Gamma = 0$) corresponds to the Fe III concentration that completely suppresses the 652 nm peak (i.e. 42 mM in this case): for larger Fe III concentrations, the reaction pH is low enough in order to completely inhibit the dye formation. The proposed model can only be applied for Fe III concentrations below the aforementioned Fe III concentration that completely inhibits the dye production, and the extrapolation to higher Fe III concentrations has no physical meaning.

The obtained interference model can be used to estimate the relative error in the ammonia quantification using the salicylate method, due to the presence of Fe III in the sample (Fig. 4). The presence of Fe III in the sample is not harmful from the ammonia quantification perspective for low Fe III concentrations and large TAN concentrations (white region in Fig. 4). In these cases, the relative error in ammonia quantification due to Fe III presence in the sample is lower than the experimental error (i.e. 5%). For samples with low TAN concentrations and large Fe III concentrations, the background increase causes an overestimation of the TAN concentration in the sample; whereas for samples with high TAN and Fe III concentrations, the interference effects overcomes the background increase, resulting in an underestimation of the real TAN concentration in the sample.

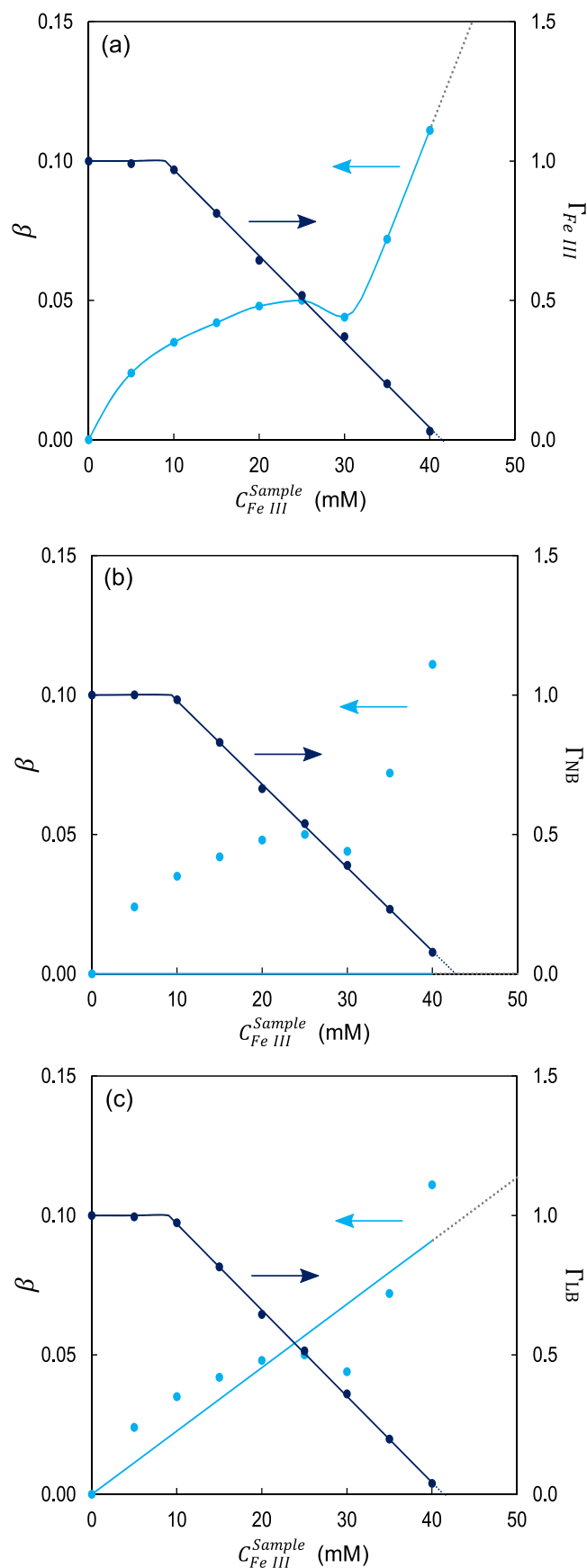


Figure 3. Background and interference coefficients (β and Γ respectively), calculated using the real background curve (a), and with the "no background" (b) and the "linear background" (c) approximations. The dots correspond to the points calculated from the experimental spectra; the continuous lines corresponds to the fitted empirical models; and the dotted lines corresponds to the extrapolation of the fitted models. First, the experimental background coefficients were calculated using the spectra from Fig. 2a and Eq. 2. In the case of the real background (a), the experimental data were interpolated by a cubic spline; for the "No background" approximation (b), a $\beta = 0$ model was used; and for the "Linear background" approximation (c), the experimental β values were fitted to a linear model. Second, the associated interference coefficients were calculated from Fig. 2b, using Eq. 3 and the real background values for the real background curve (a); Eq. 6 for the "No background" approximation (b); and Eq. 8 and the fitted linear background model for the "Linear background" approximation (c). The obtained interference coefficients were fitted to model (4). The parameters of the fitted models are given in Table I.

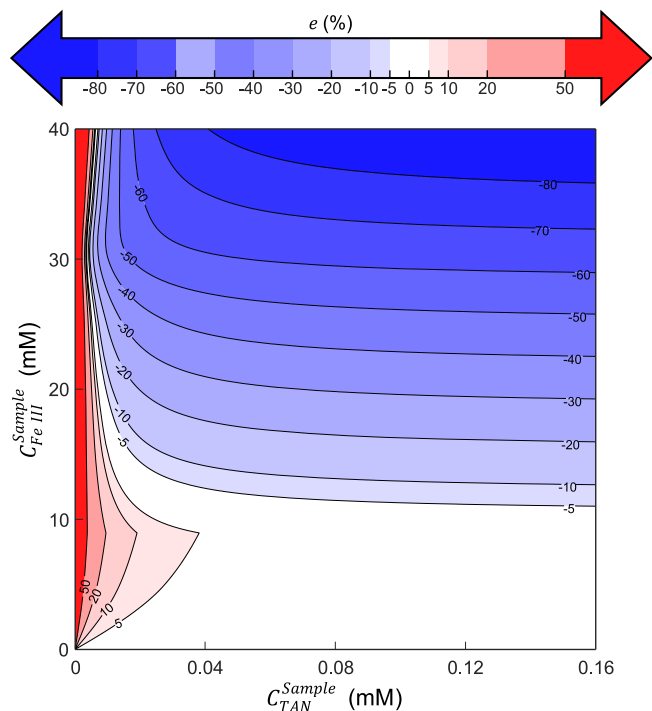


Figure 4. Prediction, using the proposed fitted empirical interference model, of the relative error (e , in %) in the ammonia quantification using the salicylate method, due to the presence of Fe III in the sample, as a function of the TAN and Fe III concentrations in the sample. The white zone identifies the locus of the C_{TAN}^{Sample} – $C_{Fe III}^{Sample}$ plane in which the relative error in the ammonia quantification due to the presence of Fe III in the sample is lower than the experimental error (i.e. $\pm 5\%$). Red regions are regions of the C_{TAN}^{Sample} – $C_{Fe III}^{Sample}$ plane, in which the Fe III presence causes the salicylate method to overestimate the real ammonia concentration in the sample (i.e. positive relative errors); whereas the blue zones are regions of C_{TAN}^{Sample} – $C_{Fe III}^{Sample}$ plane, in which the Fe III presence causes the salicylate method to underestimate the real ammonia concentration in the sample (i.e. negative relative errors).

The presence of Fe III in the sample can lead to relative errors in ammonia quantification larger than 80%! This result justifies the need of a correction method, in case that the analyzed sample is out of the white zone.

Correction method for correcting the Fe III interferences on the salicylate method.—If the Fe III concentration in a given sample is known, the empirical model proposed earlier, can be used to calculate the interference coefficient, which can then be used as a correction factor to correct the Fe III interference effect. Clearing the TAN concentration from Eq. 1:

$$C_{TAN}^{Sample} = \frac{A_{652nm}(C_{TAN}^{Sample}, C_{Fe III}^{Sample}) - \beta(C_{Fe III}^{Sample})}{l \cdot \varepsilon_{652nm}^{*}(C_{Fe III}^{Sample} = 0) \cdot \Gamma(C_{Fe III}^{Sample})} \quad [5]$$

Where $\varepsilon_{652nm}^{*}(C_{Fe III}^{Sample} = 0)$ is obtained from the calibration curve in water samples (Fig. 1a). $\beta(C_{Fe III}^{Sample})$ is calculated from the background curve (Fig. 2a), and $\Gamma(C_{Fe III}^{Sample})$ is calculated using the empirical model proposed above, which requires to first obtain the interference curve (Fig. 2b) in order to obtain the experimental interference coefficients and then fit the empirical model. Once these 3 parameters are known, the above expression can be used to estimate the TAN concentration in a given sample from its measured absorbance at 652 nm, $A_{652nm}(C_{TAN}^{Sample}, C_{Fe III}^{Sample})$. In this way, the Fe III interference on the salicylate method is corrected.

As explained in the previous section, the empirical model is only applicable to Fe III concentrations below the Fe III concentration that suppresses totally the dye generation. Consequently, the

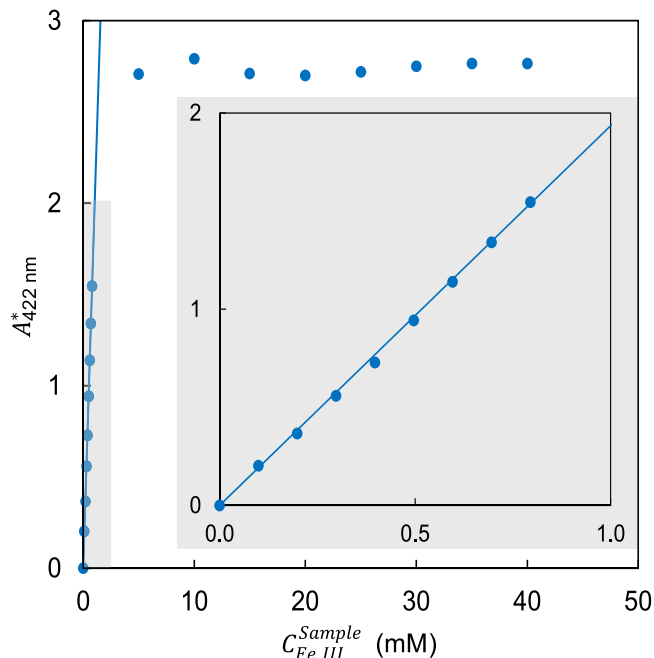


Figure 5. The absorbance of the 422 nm peak (A_{422nm}) in the UV–Visible spectra as a function of the Fe III concentration ($C_{Fe III}^{Sample}$) obtained by using the salicylate method on samples with different Fe III concentrations and a TAN concentration of 0.12 mM. The dots correspond with the experimental points, whereas the line corresponds to the linear regression line fitted to the low concentration linear zone. From the slope of the fitted line, and the optic path of the used cuvettes ($l = 1$ cm), the effective molar attenuation coefficient was determined: $\varepsilon^{*} = 1.9 \text{ mM}^{-1} \cdot \text{cm}^{-1}$ ($R^2 = 99.91\%$). Inset: Low Fe III concentration zoom.

proposed correction method cannot be applied to samples with an Fe III concentration larger than the aforementioned concentration (i.e. around 42 mM in this case). In samples with a larger Fe III concentration, the peak is totally suppressed, and therefore, correcting the interference effect is not possible without first diluting the sample prior to applying the salicylate method.

Using the described correction method, once the 3 curves (i.e. the calibration curve in water samples, the background curve and the interference curve) are obtained experimentally, the Fe III interference can be corrected in any sample (with an Fe III concentration below 42 mM). This is a great advantage of this correction method in comparison with the experimental correction method (i.e. obtaining the calibration curve in the presence of the corresponding Fe III concentration): with the proposed correction method, only 3 curves have to be experimentally obtained in order to correct the interference effect in all the samples; whereas, with the traditional experimental correction method, a different calibration curve has to be experimentally obtained for each sample with a different Fe III concentration. Of course, this advantage is decisive only in cases where the Fe III concentration changes significantly from sample to sample.

Two distinct trends with the Fe III concentration can be identified in the absorbance of the 422 nm peak of the samples containing Fe III analyzed using the salicylate method (Fig. 5): for low Fe III concentrations, the 422 nm peak grows linearly with the Fe III concentration; whereas, for high Fe III concentrations, the 422 nm peak reaches saturation (i.e. instrument maximum), and remains constant with further increases of the Fe III concentration. The fact that this spectrum feature is related to the Fe III concentration in the sample is consistent with the fact that this peak is related to colored Fe compounds, such as $\text{Fe}(\text{OH})_3$ and Fe–Salicylate complex(es). Due to the linear relation between the 422 nm peak absorbance and the Fe III concentration in the sample, this peak can be used to quantify the Fe III concentration in the sample.

This suggests that the interference correction method proposed in this work can be used to implement an autocorrective method in which the interference could be corrected with the UV–Visible spectrum itself: the (unknown) Fe III concentration in the sample would be quantified using the 422 nm peak, and then, the interference correction method would be applied in order to correct the effect of the Fe III interference. The problem is that the linearity region of the Fe III quantification peak only extends to Fe III concentrations up to around 1 mM (Fig. 5); while the Fe III interference is only significant above the threshold concentration of around 10 mM (Fig. 3a). This means that for the Fe III concentrations for which the interference is significant (i.e. where the correction is required), the 422 nm peak saturates and therefore cannot be used to quantify the Fe III concentration. It is true that the saturation value depends on the UV–Visible instrument used to perform the measurements: so, maybe with an instrument with a higher saturation value, the 422 nm peak would not saturate in the 10 mM–40 mM range. However, even assuming that the Beer–Lambert law holds in the aforementioned Fe III concentration range, with an effective molar attenuation coefficient of around $1.9 \text{ mM}^{-1} \cdot \text{cm}^{-1}$, the absorbance for a concentration of 10 mM would be of around 19, and the absorbance for a concentration of 40 mM would be greater than 75. Nowadays UV–Visible spectrophotometers can measure reliably absorbances up to 3; and some very advanced instruments are able to measure absorbances up to 10.⁵¹ A possible solution to this problem is to use cuvettes with shorter light paths: for instance, assuming a maximum absorbance of 3 due to instrument limitations, an optic path of 0.39 mm would be required for measuring Fe III concentrations up to 40 mM. Such special cells can be found in the market, however they are particularly expensive. So, with the UV–Visible technology available today, an autocorrective method is very difficult (and costly) to implement.

The interference correction method can be used to implement two other correction methods, in order to overcome the limitation of the autocorrective method: a semi-autocorrective method and a non-autocorrective method. On the one hand, in the semi-autocorrective method, the sample is measured using the salicylate method, then diluted accordingly (so that the 422 nm peak falls in its linear region) and remeasured. Since the 422 nm peak position is very pH sensitive, it is important not to change the pH of the sample during the dilution process. Because of this, the dilution should be done by adding solution S2 (i.e. 340 mM sodium citrate and 465 mM sodium hydroxide solution) to the sample. From the 422 nm peak of the second measurement (i.e. diluted sample), the Fe III concentration in the original sample is determined. And then, the result is used to correct using the interference correction method the first measurement (i.e. non-diluted sample), obtaining the TAN concentration in the sample. On the other hand, in the non-autocorrective method, each sample is divided into two aliquots. The first one is measured using the salicylate method, while the second one is used to measure the Fe III concentration using an Fe III quantification method such as the ferrozine method,⁵² the desferal-phenanthroline method,⁵³ flame atomic absorption spectrophotometry,⁵⁴ ion chromatography spectrophotometry⁵⁵ or ICP (Inductively Coupled Plasma) spectroscopy.⁵⁶ The salicylate measurement is corrected using the interference correction method, using the measured Fe III concentration.

From the three experimental curves required to apply the correction method, the calibration curve in water samples and the interference curve are completely necessary: without them, the correction method cannot be used. However, since the background levels are relatively low (Fig. 2a), two different approximations can be used in order to avoid having to obtain the whole background curve, reducing in this way the total number of required experimental measurements to use the correction method. The first approximation that can be considered is the “No background” approximation: the background is assumed to be low enough to be considered as 0. In this approximation, the background coefficient is considered as 0, for every Fe III concentration. Using Eq. 3, the

interference coefficient considering the “No background” approximation, Γ_{NB} , can be calculated as:

$$\Gamma_{NB}(C_{Fe\text{ III}}^{\text{Sample}}) = \frac{A_{652\text{ nm}}(C_{TAN}^{\text{Sample}}, C_{Fe\text{ III}}^{\text{Sample}})}{A_{652\text{ nm}}(C_{TAN}^{\text{Sample}}, C_{Fe\text{ III}}^{\text{Sample}} = 0)} \quad [6]$$

The second approximation that can be considered is the “Linear background” approximation: the background is assumed to increase linearly with the Fe III concentration. Therefore, the background coefficient assuming the “Linear background” approximation, β_{LB} , is given by:

$$\beta_{LB}(C_{Fe\text{ III}}^{\text{Sample}}) = \alpha \cdot C_{Fe\text{ III}}^{\text{Sample}} \quad [7]$$

Where α is the slope that can be obtained by fitting the background curve to the linear model (7). Once α is known, the interference coefficient considering the “Linear background” approximation, Γ_{LB} , can be calculated as:

$$\Gamma_{LB}(C_{Fe\text{ III}}^{\text{Sample}}) = \frac{A_{652\text{ nm}}(C_{TAN}^{\text{Sample}}, C_{Fe\text{ III}}^{\text{Sample}}) - \beta_{LB}(C_{Fe\text{ III}}^{\text{Sample}})}{A_{652\text{ nm}}(C_{TAN}^{\text{Sample}}, C_{Fe\text{ III}}^{\text{Sample}} = 0)} \quad [8]$$

The “Linear background” approximation is able to fit relatively well (with a determination coefficient above 80%), the real background (Fig. 3c). This implies that although the real background curve displays a complex trend due to pH variations that shift the position of the spectrum feature, it can be modelled quite well by a linear model. Furthermore, the interference coefficients obtained using these approximations display the same trends than the real interference coefficients (Figs. 3b and 3c). Therefore, the empirical model proposed to model the effect of the Fe III concentration on the real interference coefficient (Eq. 4), can also be used for the interference coefficients obtained for the two approximations. In fact, the determination coefficient of the fitted interference coefficient models is above 99.95% both, for the “No background” approximation and the “Linear background” approximation (Table I).

For high TAN concentrations and low Fe III concentrations, these approximations give good results (i.e. low relative errors) (Fig. 6). On the contrary, for low TAN concentrations and high Fe III concentrations, the approximations yield quantification results with very high relative errors (Fig. 6). Moreover, for a given sample (i.e. given TAN and Fe III concentrations), the “Linear background” gives better estimations (i.e. lower error) than the “No background” approximation (Figs. 6a and 6b). The great advantage of the “No background” approximation is that it does not require any background measurement at all. Meanwhile, the “Linear background” approximation is an intermediate solution since it requires only one background measurement, instead of the whole background curve. These results show that the background curve can be spared (reducing the total number of experimental measurements) for samples with low Fe III concentrations and high TAN concentrations. Figure 6 allows one to quantitatively decide if the whole background curve (i.e. real background) is required, if only one background measurement (i.e. “Linear background” approximation) is needed, or if no background measurement is needed at all (i.e. “No background” approximation), as a function of the required accuracy (i.e. maximum allowable error) and the TAN and Fe III concentrations of the sample.

Conclusions

The presence of Fe III ions in the sample causes a strong negative interference on the ammonia quantification peak of the salicylate method. This interference is due to the sequestration by the Fe III ions of the hydroxide ions that are added with the salicylate reagents in order to increase the pH of the mixture until its optimum value for the dye formation reaction. The reduction of the reaction pH inhibits the dye formation reaction, causing a decrease in the dye production

Table I. Fitted parameters of the background and interference models. First, the experimental background coefficients were calculated using the spectra from Fig. 2a and Eq. 2. In the case of the real background, the experimental data were interpolated by a cubic spline; for the “No background” approximation, a $\beta = 0$ model was used; and for the “Linear background” approximation, the experimental β values were fitted to a linear model. Second, the associated interference coefficients were calculated from Fig. 2b, using Eq. 3 and the real background values for the real background model; Eq. 6 for the “No background” approximation; and Eq. 8 and the fitted linear background model for the “Linear background” approximation. The obtained interference coefficients were fitted to model (4). The model has 2 parameters: $C_{\text{threshold}}$ and δ . The first, corresponds with the threshold Fe III concentration below which there is no interference. The second, quantifies the interference effect magnitude. The determination coefficient (R^2) of each one of the fitted models is also presented, as a quantifier of the goodness of fit.

	β model	Γ model		
		$C_{\text{threshold}}$ (mM)	δ (M^{-1})	R^2 (%)
Real background	Cubic spline interpolation $R^2 = 1$	8.96	30.8	99.90
“No background” approximation	$\beta = 0$ $R^2 = -$	9.33	29.9	99.96
“Linear background” approximation	$\beta = 2.27 \cdot \frac{C_{\text{Fe III}}^{\text{Sample}}}{M}$ $R^2 = 80.76\%$	9.02	30.9	99.96

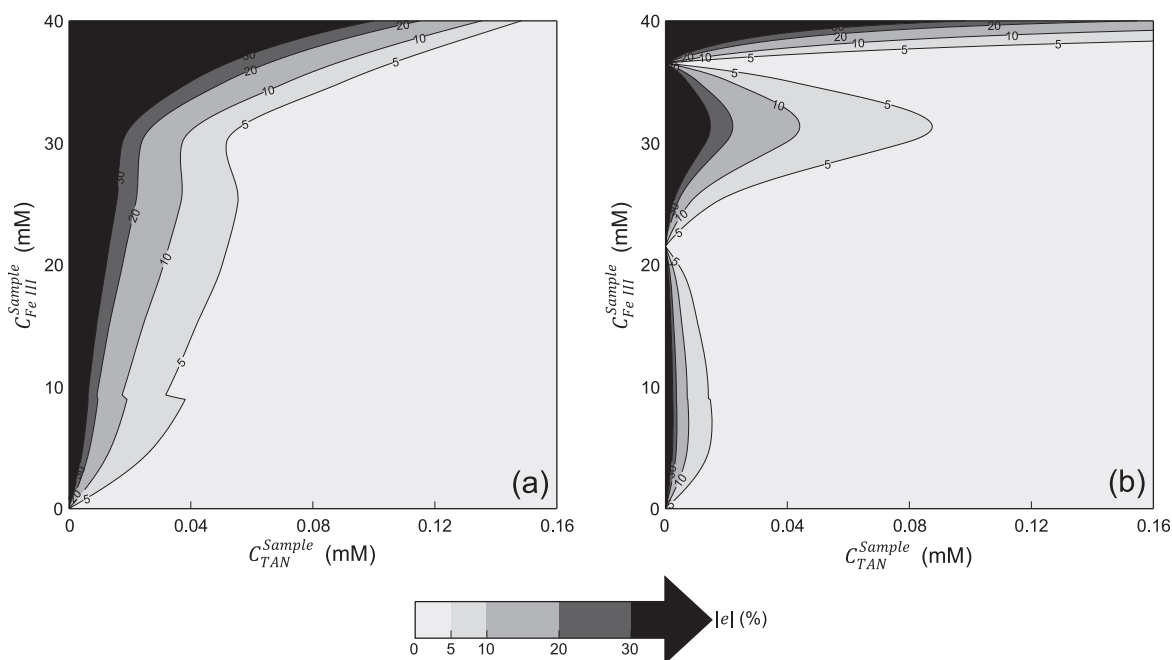


Figure 6. Absolute value of the relative error ($|e|$, expressed in %) in the ammonia concentration calculated using the proposed correction method when the “No background” approximation (a) or the “Linear background” approximation (b) are considered, rather than using the real background curve.

yield. The Fe III interference only is significant above a threshold Fe III concentration of 10 mM. For Fe III concentrations above 42 mM, the dye production is totally inhibited, and the indophenol peak is totally suppressed.

In this work, an interference model of the Fe III interference on the salicylate method has been proposed. This model can be used to correct the effect of the Fe III interference on the ammonia quantification by the salicylate method. The correction method requires obtaining three curves experimentally: the calibration curve in water samples, the background curve and the interference curve. Once these three curves are available, the Fe III interference can be corrected in any sample, with an Fe III concentration below 42 mM. When a batch of samples presents a great Fe III concentration variability, this is a great advantage over the actual experimental correction method, since with only three experimental curves the correction can be done for all the samples; whereas, the experimental correction method requires to obtain a different experimental calibration curve for every Fe III concentration. Moreover, the

background curve can be spared (reducing the total number of experimental measurements) for samples with low Fe III concentrations and high TAN concentrations: a quantitative criterion for deciding whether the whole background curve is required or not, based on the required accuracy (i.e. maximum allowable error) and the TAN and Fe III concentrations of the sample is presented in this work.

The interference correction method proposed in this work can be used in two ways. On the one hand, it can be used as a semi-autocorrective method: the sample is measured using the salicylate method, then diluted accordingly and remeasured. The 422 nm peak of the diluted sample is used to obtain the Fe III concentration in the original sample; which is then used to correct the measurement of the non-diluted sample with the interference correction method. On the other hand, the interference correction method can be used as a non-autocorrective method: each sample is divided into two aliquots, one of which is analyzed using the salicylate method, while the other one is analyzed using an Fe III quantification method. Then, the

salicylate measurement is corrected using the interference correction method, with the measured Fe III concentration.

Acknowledgments

This work was supported by the Toyota Research Institute through the Accelerated Materials Design and Discovery program. This work made use of the MRSEC Shared Experimental Facilities at MIT (SEM) supported by the National Science Foundation under award number DMR-1419807 as well as the HZDR Ion Beam Center TEM facilities. J.J.G.S. is very grateful to the Generalitat Valenciana and to the European Social Fund, for their economic support in the form of Vali+d postdoctoral grant (APOSTD-2018-001). G.M.L. was partially supported by a Natural Sciences and Engineering Research Council of Canada (NSERC) PGS-D.

Author Contributions

The manuscript was written through contributions of all authors. All authors have given approval to the final version of the manuscript.

ORCID

Juan José Giner-Sanz  <https://orcid.org/0000-0003-0441-6102>

Graham M. Leverick  <https://orcid.org/0000-0001-8541-4381>

Yang Shao-Horn  <https://orcid.org/0000-0001-8714-2121>

References

1. J. Kibsgaard, J. Nørskov, and I. Chorkendorff, *ACS Energy Lett.*, **4**, 2986 (2019).
2. Q. Wang, J. Guo, and P. Chen, *Joule*, **4**, 705 (2020).
3. Y. Wang et al., *Angew. Chem. Int. Edit.*, **58**, 9464 (2019).
4. S. Andersen et al., *Nature*, **570**, 504 (2019).
5. K. Kim, N. Lee, C. Yoo, J. Kim, H. Yoon, and J. Han, *J. Electrochem. Soc.*, **163**, F610 (2016).
6. K. Kim, C. Yoo, J. Kim, H. Yoon, and J. Han, *J. Electrochem. Soc.*, **163**, F1523 (2016).
7. T. Murakami, T. Nishikiori, T. Nohira, and Y. Ito, *J. Electrochem. Soc.*, **152**, D75 (2005).
8. B. Liu, A. Yasin, T. Musho, J. Bright, H. Tang, L. Huang, and N. Wu, *J. Electrochem. Soc.*, **166**, H3091 (2019).
9. J. Yang, T. Li, C. Zhong, X. Guan, and C. Hu, *J. Electrochem. Soc.*, **163**, E288 (2016).
10. P. Wang, F. Chang, W. Gao, J. Guo, G. Wu, T. He, and P. Chen, *Nature Chem.*, **9**, 64 (2017).
11. J. Nash, X. Yang, J. Anibal, J. Wang, Y. Yan, and B. Xu, *J. Electrochem. Soc.*, **164**, F1712 (2017).
12. Q. Wang, J. Guo, and P. Chen, *J. Energ. Chem.*, **36**, 25 (2019).
13. M. P. E. Berthelot and R. de Chimie, *Appliquée*, **1**, 284 (1859).
14. D. Li, X. Xu, Z. Li, T. Wang, and C. Wang, *Trend. Anal. Chem.*, **127**, 115890 (2020).
15. P. Searle, *Analyst*, **109**, 549 (1984).
16. Y. Song et al., *Science Adv.*, **4**, 1700336 (2018).
17. I. Ivancic and D. Degobbi, *Water Res.*, **18**, 1143 (1984).
18. O. Ayyub, A. Behrens, B. Heligman, M. Natoli, J. Ayoub, G. Cunningham, M. Summar, and P. Kofinas, *Mol. Genet. Metab.*, **115**, 95 (2015).
19. M. Prieto-Blanco, N. Jornet-Martínez, J. Verdú-Andrés, C. Molíns-Legua, and P. Campíns-Falcó, *Talanta*, **198**, 371 (2019).
20. M. Prieto-Blanco, N. Jornet-Martínez, Y. Moliner-Martínez, C. Molíns-Legua, R. Herráez-Hernández, J. Verdú-Andrés, and P. Campíns-Falcó, *Sci. Total Environ.*, **503**, 105 (2015).
21. M. Prieto-Blanco, A. Ballester-Caudet, F. Souto-Varela, P. López-Mahía, and P. Campíns-Falcó, *Environ. Pollut.*, **265**, 114911 (2020).
22. J. McEnaney, S. Blair, A. Nielander, J. Schwalbe, D. Koshy, M. Cargnello, and T. Jaramillo, *ACS Sustainable Chem. Eng.*, **8**, 2672 (2020).
23. Z. Schiffer, N. Lazouski, N. Corbin, and K. Manthiram, *J. Phys. Chem. C*, **123**, 9713 (2019).
24. Y. Moliner-Martínez, R. Herráez-Hernández, and P. Campíns-Falcó, *Anal. Chim. Acta*, **534**, 327 (2005).
25. C. Pasquali, P. Hernando, and J. Alegria, *Anal. Chim. Acta*, **600**, 177 (2007).
26. H. Kashima and J. Regan, *Environ. Sci. Tech.*, **49**, 3195 (2015).
27. A. Caballo-López and M. Luque de Castro, *Anal. Chem.*, **78**, 2297 (2006).
28. J. Bietz, *Anal. Chem.*, **46**, 1617 (1974).
29. N. Lazouski, Z. Schiffer, K. Williams, and K. Manthiram, *Joule*, **3**, 1127 (2019).
30. J. McEnaney, A. Singh, J. Schwalbe, J. Kibsgaard, J. Lin, M. Cargnello, T. Jaramillo, and J. Nørskov, *Energ. Environ. Sci.*, **10**, 1621 (2017).
31. A. Cerda, M. Oms, R. Forteza, and V. Cerda, *Anal. Chim. Acta*, **311**, 165 (1995).
32. C. Molíns-Legua, S. Meseguer-Lloret, Y. Moliner-Martínez, and P. Campíns-Falcó, *Trend. Anal. Chem.*, **25**, 282 (2006).
33. H. Verdouw, C. V. Ehteld, and E. Dekkers, *Water Res.*, **12**, 399 (1978).
34. A. Kempers and C. Kok, *Anal. Chim. Acta*, **221**, 147 (1989).
35. D. Li, Z. Li, C. Wang, T. Wang, and X. Xu, *Spectroscopic method for the detection and Determination of Ammonia Nitrogen in Aquaculture Water, Spectroscopic Tools for Food Analysis* (IOP Publishing Ltd., United Kingdom) (2019).
36. H. Yu, L. Yang, D. Li, and Y. Chen, *Inform. Process. Agr.*, (2020).
37. C. Wang, Z. Lia, Z. Pand, and D. Li, *Comp. Electron. Agr.*, **150**, 364 (2018).
38. C. Fernandez, N. Hortance, Y. Liu, J. Lim, K. Hatzell, and M. Hatzell, *J. Mat. Chem. A*, **8**, 15591 (2020).
39. Hach Company, *Hach Water Analysis Handbook* (Loveland, Colorado) (1992).
40. J. Guo and P. Chen, *Chem.*, **3**, 709 (2017).
41. A. Sclafani, V. Augugliaro, and M. Schiavello, *J. Electrochem. Soc.*, **130**, 734 (1983).
42. F. Zhou, L. Azofra, M. Ali, M. Kar, A. Simonov, C. McDonnell-Worth, C. Sun, X. Zhang, and D. MacFarlane, *Energ. Environ. Sci.*, **10**, 2516 (2017).
43. M. McDonald, J. Fuller, A. Fortunelli, W. Goddard, and Q. An, *J. Phys. Chem. C*, **123**, 17375 (2019).
44. S. Chen, S. Perathoner, C. Ampelli, C. Mebrahtu, D. Su, and G. Centi, *Angew. Chem. Int. Edit.*, **56**, 2699 (2017).
45. H. Wang et al., *ACS Catal.*, **10**, 4914 (2020).
46. C. Bower and T. Holm-Hansen, *Can. J. Fish. Aquat. Sci.*, **37**, 794 (1980).
47. P. Le and C. Boyd, *J. World Aquacult. Soc.*, **43**, 885 (2012).
48. D. Lide, *CRC Handbook of Chemistry and Physics* (CRC Press, Boca Raton) 85th ed. (2005).
49. R. Every-Pym and P. Millham, *Anal. Chem.*, **48**, 1413 (1976).
50. M. Krom, *Analyst*, **105**, 305 (1980).
51. Shimadzu Corporation, *UV-vis spectrophotometers. UV-2600 and UV-2700. Instrument specifications* (Metropolis, Tokyo) (2011).
52. E. Viollier, P. Inglett, K. Hunter, A. Roychoudhury, and P. Van Cappellen, *Appl. Geochem.*, **15**, 785 (2000).
53. D. Yegorov, A. Kozlov, O. Azizova, and Y. Vladimirov, *Free Radical Bio. Med.*, **15**, 565 (1993).
54. H. Bag, A. Turker, A. Tunçell, and M. Lale, *Anal. Sci.*, **17**, 901 (2001).
55. H. Kaasalainen, A. Stefánsson, and G. Druschel, *Int. J. Environ. Anal. Chem.*, **96**, 1074 (2016).
56. X. Pu, B. Hu, Z. Jiang, and C. Huang, *Analyst*, **130**, 1175 (2005).